# Molecular Fingerprint of Endocannabinoid Signaling in the Developing Paraventricular Nucleus of the Hypothalamus as Revealed by Single-Cell RNA-seq and in situ Hybridization

Evgenii Tretiakov [†], Zsófia Hevesi [†], Csenge Böröczky, Alán Alpár, Tibor Harkany [*], Erik Keimpema [*]

Posted Date: 2 May 2025

doi: 10.20944/preprints202505.0066.v1

Keywords: cannabinoid receptor; endocannabinoid; hypothalamus; postnatal development; monoacylglycerol lipase; sn-1-diacylglycerol lipase

 doi:10.20944/preprints202505.0066.v1



*Article*

# Molecular Fingerprint of Endocannabinoid Signaling in the Developing Paraventricular Nucleus of the Hypothalamus as Revealed by Single-Cell RNA-seq and in situ Hybridization

**Evgenii Tretiakov [1,†], Zsófia Hevesi [1,†], Csenge Böröczky [1], Alán Alpár [2,3], Tibor Harkany [1,4,*] and Erik Keimpema [1,*]**

[1] Department of Molecular Neurosciences, Center for Brain Research, Medical University of Vienna, Vienna and Austria.

[2] Department of Anatomy, Histology and Embryology.

[3] SE NAP Research Group of Experimental Neuroanatomy and Developmental Biology, Semmelweis University, Budapest, Hungary.

[4] Department of Neuroscience, Biomedicum 7D, Karolinska Institutet, Solna, Sweden.

* Correspondence: Tibor.Harkany@ki.se (T.H.); Erik.Keimpema@meduniwien.ac.at (E.K.)

Dr. Erik Keimpema (*Tel.:* +43 1 40160 34063) or Dr. Tibor Harkany (*Tel.:* +43 1 40160 34050) both at the Department of Molecular Neurosciences, Center for Brain Research, Medical University of Vienna, Vienna, Austria.

† These authors contributed equally.

**Abstract:** The paraventricular nucleus of the hypothalamus (PVN) regulates, among others, the stress response, sexual behavior, and energy metabolism, through its magnocellular and parvocellular neurosecretory cells. Within the PVN, ensemble coordination occurs through the many long-range synaptic afferents, whose activity in time relies on retrograde neuromodulator by, e.g., endocannabinoids. However, the nanoarchitecture of endocannabinoid signaling in the PVN, especially during neuronal development, remains undescribed. By using single-cell RNA sequencing, in situ hybridization, and immunohistochemistry during fetal and postnatal development in mice, we present a spatiotemporal map of both the 2-arachydonoylglycerol and anandamide signaling cassettes, with a focus on receptors and metabolic enzymes, in both molecularly-defined neurons and astrocytes. We find type 1 cannabinoid receptors (*Cnr1*), but neither *Cnr2* nor *Gpr55*, expressed only in neurons of the PVN. A developmental switch from *Daglb* to *Dagla* is observed, with minimal *Mgll* mRNA in all neuronal subtypes of the PVN. Notably, astrocytes also expressed both *Dagl* isoforms. *Napepld*, and *Faah* were sparsely present. Immunohistochemistry validated mRNA expression, and suggested that endocannabinoid signaling is configured to modulate the activity of afferent inputs, rather than local neurocircuits, in the PVN.

**Keywords:** cannabinoid receptor; endocannabinoid; hypothalamus; monoacylglycerol lipase; postnatal development; *sn*-1-diacylglycerol lipase

## 1. Introduction

The hypothalamus is an archetypical, evolutionary conserved vertebrate brain structure that controls essential physiological processes, including food and fluid intake, energy homeostasis, stress responses, sleep/wake cycles, as well as sexual behavior and reproduction, to ensure the subject's survival[1]. Consequently, the hypothalamus contains a collection of topographically segregated neuronal loci, each possessing their own molecular signature and synaptic connectivity. For instance, the paraventricular nucleus (PVN), flanking the third ventricle bilaterally, and mainly consisting of excitatory vesicular glutamate transporter 2 (*Slc17a6*/VGLUT2)$^+$ neurons (**Figure 1a**), integrates

 doi:10.20944/preprints202505.0066.v1



neuroendocrine and autonomic functions through its dorsolateral magnocellular and medioventral parvocellular subdivisions. Its neurosecretory magnocellular cells are large-bodied neurons expressing either vasopressin ($m^{AVP}$) or oxytocin ($m^{OXT}$), with both subpopulations projecting directly to the posterior pituitary, where they release their hormones directly into the systemic circulation to regulate blood pressure, water-balance, and maternal, social and feeding behaviors, respectively[2]. In contrast, parvocellular (small-bodied) neurosecretory neurons contain corticotrophin-releasing hormone (CRH; $p^{CRH}$), thyrotropin-releasing hormone (TRH; $p^{TRH}$), or somatostatin (SST; $p^{SST}$) and extend their axons to the median eminence, a gateway structure for hypothalamic hormones to reach the anterior pituitary through the hypophyseal portal system. Once released into the portal blood, CRH orchestrates the hypothalamus-pituitary-adrenal (HPA) axis upon stress, with sequential release events for adrenocorticotropic hormone (ACTH) from the pituitary, and cortisol from the adrenal cortex. TRH stimulates the release of thyroid-stimulating hormone (TSH) from the anterior pituitary, thus controlling metabolic and cardiovascular function through the hypothalamus-pituitary-thyroid (HPT) axis. Antagonistically, SST inhibits the release of TSH from the anterior pituitary[3]. Thus, the PVN is essential for bodily metabolism with its dysfunction implicated in obesity, hypertension, diabetes insipidus[2], as well as anxiety and depression[4,5].

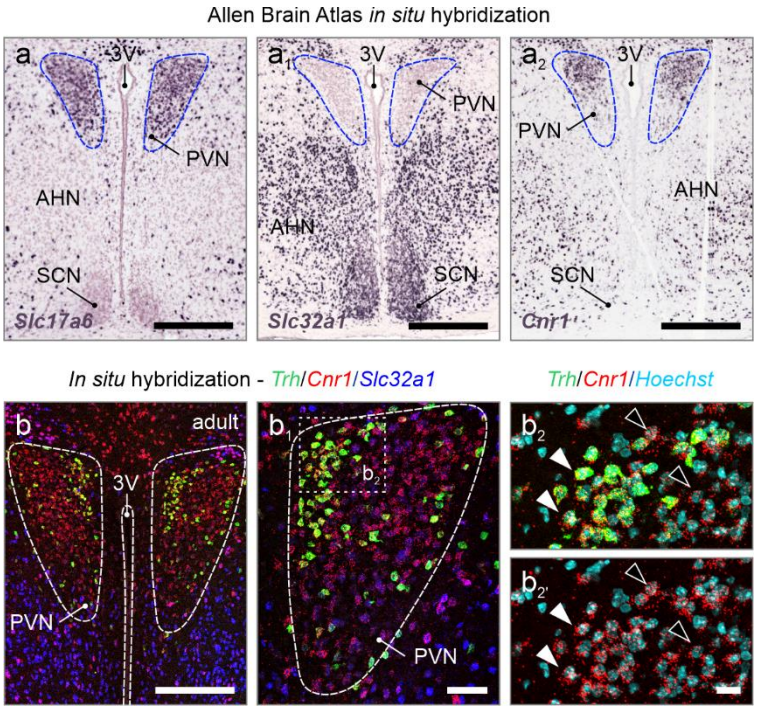


**Figure 1. *Cnr1* mRNA expression in the adult mouse PVN.** (**a-a$_2$**) Open-source in situ hybridization data from the Allen Brain Atlas (https://portal.brain-map.org/) in the adult mouse PVN reveals glutamatergic (*Slc17a6*$^+$), but not GABAergic (*Slc32a1*$^+$) neurons, along with the accumulation of *Cnr1* mRNA. (**b-b$_2$**) Multiplexed in situ hybridization confirmed *Cnr1* mRNA expression in the PVN, at levels more pronounced than in neighboring regions, and *Trh*$^+$ neurons being particularly labelled (*closed* vs. *open arrowheads*). *Abbreviations:* 3V, third ventricle; AHN, anterior hypothalamic nucleus; PVN, paraventricular nucleus; SCN, suprachiasmatic nucleus. *Scale bars* = 350 μm (a-a$_3$), 200 μm (b), 50 μm (b$_1$), 20 μm (b$_2$).

To control the many physiological processes, the PVN is innervated by long-distance afferents, both excitatory and inhibitory in nature, originating from multiple brain regions: e.g., from excitatory proopiomelanocortin (POMC)$^+$/*Slc17a6*$^+$ glutamatergic[6], and inhibitory agouti-related protein (AgRP)/neuropeptide Y neurons[7] of the arcuate nucleus to control energy expenditure[8,9]; glutamatergic neurons of the amygdalo-piriform transition area, and inhibitory neurons of the central amygdala to modulate CRH secretion upon fear induction[10]; as well as inhibitory neurons of the

 doi:10.20944/preprints202505.0066.v1



bed nucleus of the stria terminals upon reward seeking and stress[11]. As a general principle, the temporal precision of both its innate neurocircuits and neuroendocrine output of the PVN is controlled by inhibitory neurotransmission originating in nearby brain areas, rather than intrinsically, through GABAA receptor-dependent inhibition[12–14]. However, synaptic integration is unlikely to be exclusively reliant on distant-positioned neurons[12,13], particularly in the absence of a major interneuron (GABA) contingent locally (**Figure 1a1,b**)[15]. Thus, we hypothesized that synaptic synchronization and local neurotransmitter availability, from both local collaterals and afferents, could additionally rely on fast-acting retrograde signaling. Indeed, compared to other hypothalamic areas, the PVN is known for its expression of type 1 cannabinoid receptor mRNA (*Cnr1*/$CB_1R$)[16], a $G_{i/o}$ protein-coupled receptor negatively affecting neurotransmitter release (**Figure 1a$_3$,b-b$_2$**). The activation of presynaptic $CB_1Rs$ occurs through 2-arachidonoylglycerol (2-AG)[17] and anandamide (AEA)[18], endocannabinoids produced in subsynaptic dendrites[19]. Indeed, engagement of CB1Rs in the PVN was shown to influence energy metabolism[20,21], food intake[20,22], and the stress response[23,24]. However, the cellular architecture of the endocannabinoid system on identified neuronal and astrocyte populations in the PVN remains unresolved, whether during development or in adulthood.

Here, we produced a comprehensive expression map of cannabinoid receptors (*Cnr1*/*Cnr2*/*Gpr55*), as well as the putative enzymes involved in 2-AG (*Dagla*/*Daglb, Mgll*) and AEA metabolism (*Napepld*/*Gde1, Faah*) at successive developmental stages. Particularly, we found that $m^{OXT}$ and $m^{AVP}$, which appear at embryonic day (E) 15.5, expressed *Cnr1*, but neither *Cnr2* nor *Gpr55*, towards postnatal day (P)21, that is pre-adolescence. Once the PVN became enriched in $p^{TRH}$/$p^{CRH}$ neurons, these neuronal subtypes also expressed *Cnr1.* Spatiotemporal *Dagla*/*Daglb* and *Mgll* expression tightly followed that of *Cnr1*, also recapitulating a robust *Daglb-to-Dagla* switch at neonatal life, in line with the predominance of DAGL$\alpha$ in retrograde neurotransmission at mature synapses[25]. For $p^{SST}$ neurons, which segregate lastly in the PVN, molecular arrangements were indistinguishable from other neuronal subtypes, yet expressional patterns were delayed as much as the emergence of $p^{SST}$ neurons themselves. *Napepld* mRNA content was minimal in all neurons, while *Faah* expression increased towards P21. Single-cell RNA-seq data showed a near complete lack of cannabinoid receptors in astrocytes of the adult PVN, but revealed *Dagla* expression. We found reliable amounts of neither *Napepld* nor *Faah* mRNA in astrocytes, reflecting previous data suggesting that astrocytes are more reliant on 2-AG signaling when interacting with nearby neurons[26,27]. In sum, we described the molecular constituents of the endocannabinoid system in identified magnocellular and parvocellular neurons, as well as astrocytes, at single-cell-precision during fetal and postnatal development of the PVN.

## 2. Results

**Neuronal diversity in the PVN during brain development.** We defined neuronal subtypes in the PVN by combining neurotransmitter and neuropeptide-related gene signatures at embryonic (E15.5-E17.5), neonatal (P0), juvenile (P2, P10), and pre-adolescent (P23) hypothalamus datasets (**Supporting Figure 1a**)[15]. At E15.5, magnocellular neurosecretory cells expressing *Oxt* ($m^{OXT}$) and *Avp* ($m^{AVP}$) mRNA appeared first, with mRNA levels gradually rising to P21 (**Figure 2a-a$_1$**). We caution that the sequence similarity between *Oxt* and *Avp* could have limited the precise assessment of *Avp* mRNA present, for which *Avp* itself was excluded for subsequent analysis[28]. Next, we distinguished parvocellular cells at E17.5, particularly $p^{CRH}$ and $p^{TRH}$ neurons, as well as a late-emerging $p^{SST}$ group after birth (**Figure 2a$_2$-a$_4$**). For parvocellular cells, mRNA levels increased as a factor of developmental stage and peaked at P10-to-P21. The temporal pattern described here was validated by an RNA-sequencing dataset published earlier[29], which also show $m^{OXT}$/$m^{AVP}$ > $p^{CRH}$/$p^{TRH}$ > $p^{SST}$ neurons, even if at shallower resolution (**Supporting Figure 1a vs. a$_1$; Supporting Figure 2a-a$_4$**). This sequence of events is compatible with the concept that long-range projection neurons of the hypothalamus mature earlier than locally-targeting neurons and/or interneurons[15].

 doi:10.20944/preprints202505.0066.v1



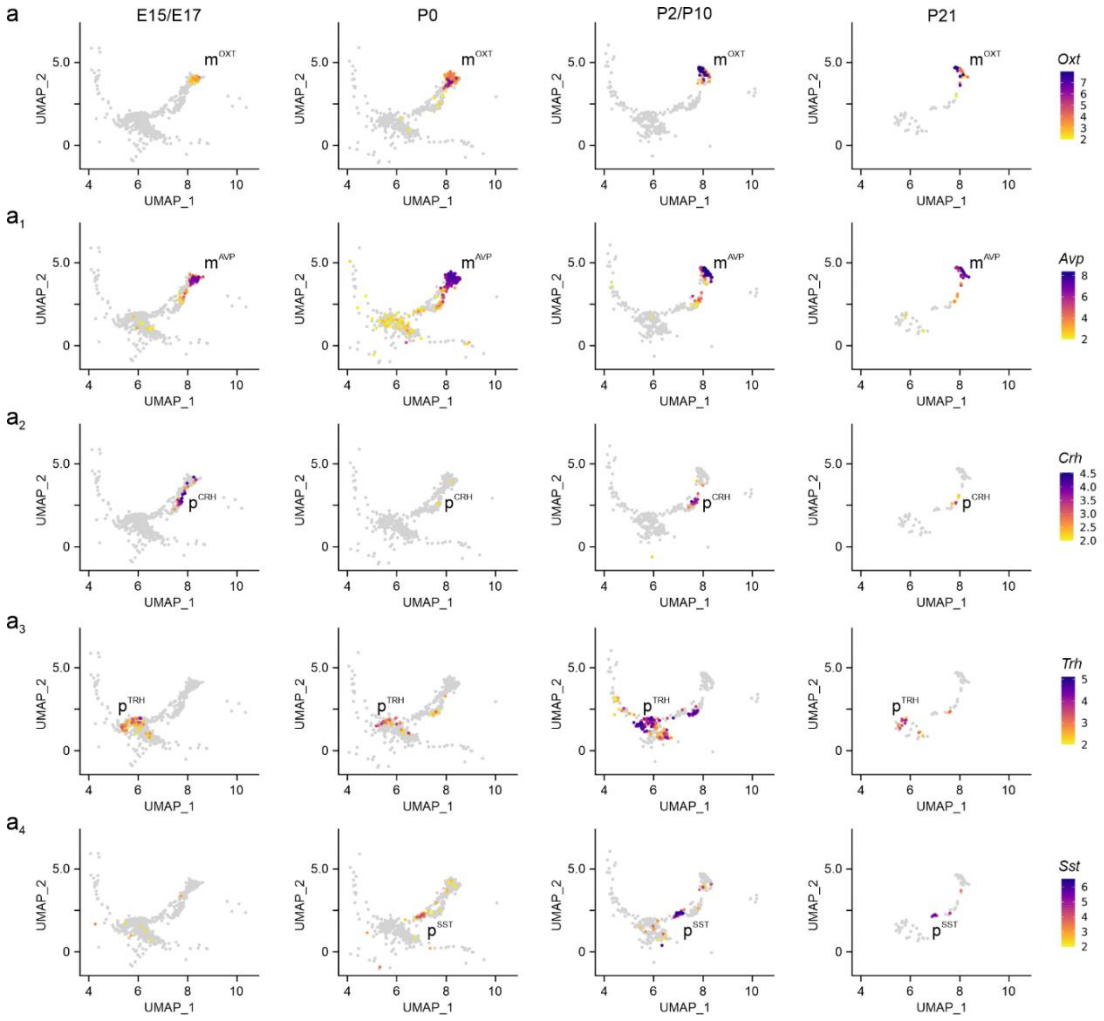


**Figure 2. Neuropeptide identifiers of the PVN.** (**a-a**$_2$) Multidimensional clustering based on neuropeptides revealed discrete magnocellular ($m^{OXT}$, $m^{AVP}$), and parvocellular cells, the latter containing *Crh*, *Trh* and *Sst* ($p^{CRH}$, $p^{TRH}$, $p^{SST}$), across successive developmental stages in the PVN. Relative expression was color-coded for each gene analyzed (to the right).

**Assembly of the endocannabinoid system.** To map genes broadly associated with the 'endocannabinoid system', we first examined gene expression for *Cnr1*, *Cnr2*[16,30], and *Gpr55*[31]. We found *Cnr1* expression at molecule numbers exceeding 3,000 per cell at E15.5 and E17.5 in subsets of $m^{OXT}$, $p^{TRH}$, and $p^{CRH}$ neurons, with its levels maintained until P21 (>1,000 mRNA copies per cell; **Figure 3a,b**). In $p^{SST}$ neurons, *Cnr1* was detected in 15-20% of cells only postnatally, correlating the temporal expression pattern of *Sst* itself (**Figure 2a**$_4$), even if in a small sample size that was not processed further. Even though *Cnr2* mRNA was previously found in the hypothalamus[32], we could not reliably detect *Cnr2* mRNA transcripts by single-cell RNA-seq in neurons, suggesting limited, if any, *Cnr2* contributions to neuronal development, at least in the PVN (**Figure 3a**$_1$). In contrast, we detected a few *Gpr55*-containing neurons, mainly $m^{OXT}$ and $p^{TRH}$ cells, with low mRNA copy numbers (<100 mRNA copies per cell) at neonatal and juvenile ages (**Figure 3a**$_2$**,b**)[33]. In sum, *Cnr1* is the main cannabinoid receptor in neurons of the PVN to respond to (endo-)cannabinoid signals, whether during axonal growth and guidance, synaptogenesis, or retrograde signaling at maturity[34].

 doi:10.20944/preprints202505.0066.v1



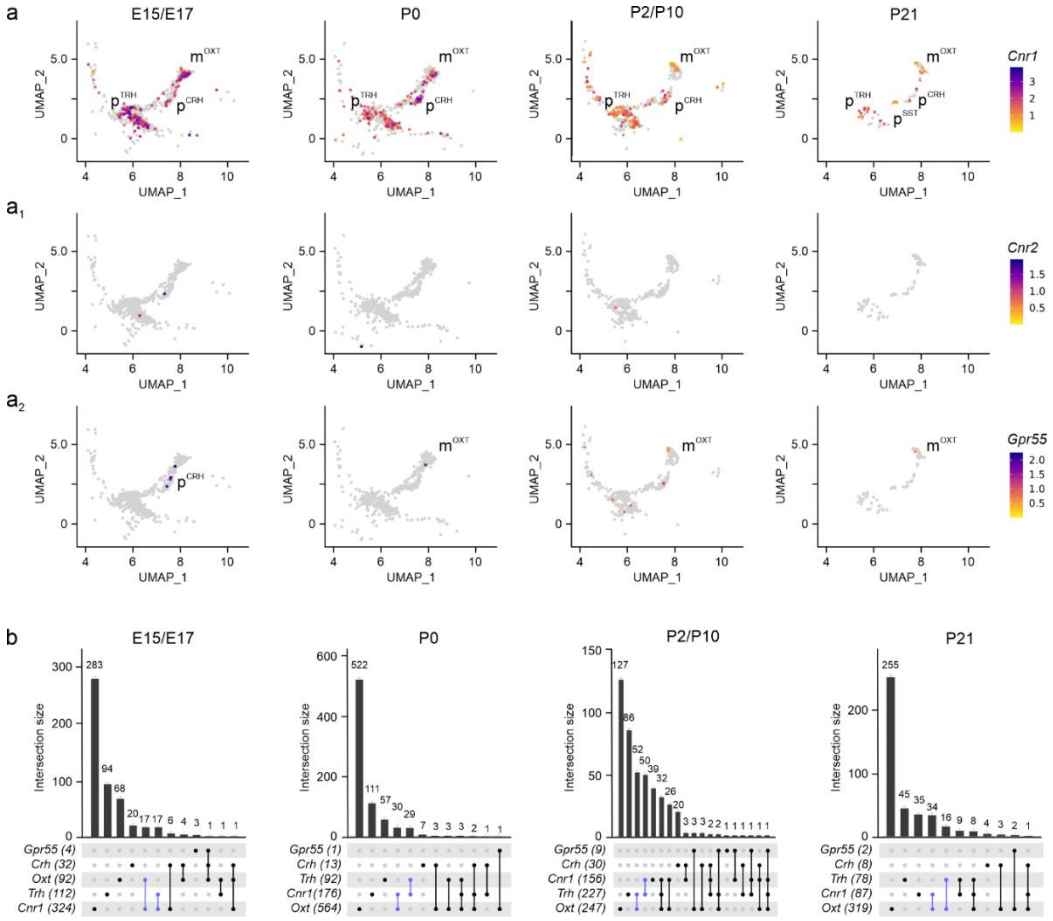


**Figure 3. Cannabinoid receptors in the PVN.** (**a-a2**) UMAP representation of cannabinoid receptors identified *Cnr1* as the dominant receptor in both magnocellular and parvocellular cells at all developmental stages analyzed, with minimal contributions from *Cnr2* (a1) and *Gpr55* (a2). Relative expression was color-coded for each gene analyzed (to the right). (**b**) *UpSet* plots showing gene enrichment and co-expression along brain development. Note the particular enrichment in $m^{OXT}$ and $p^{TRH}$ clusters (in blue), as compared to $p^{CRH}$.

Next, we assessed *Dagla*, *Daglb*[35], and *Mgll*[36] mRNA expression. Both *Dagla* and *Daglb* were found in $m^{OXT}$, $p^{TRH}$, and $p^{CRH}$ neurons at both E15.5 and E17.5, with mRNA levels, but not cell abundance, diminishing into pre-adolescence (**Figure 4a,a1,b**). Expression of *Dagla*/*Daglb* in $p^{SST}$ cells was delayed to postnatal life, as much as seen for *Cnr1* and *Sst* mRNAs (**Figure 2a4,4a**). During embryonic stages, we found a ~2.5-fold higher number of neurons expressing *Daglb*, as compared to *Dagla* (84 vs. 35 cells, over $m^{OXT}$ and $p^{TRH}$ neurons), which reversed between E17.5 and P10 (52 vs. 86 cells; **Figure 4b**), corroborating a developmental isoform switch model proposed earlier[25,35,37]. In parallel, *Mgll* expression gradually decreased towards P21. Of note, *Mgll* mRNA was found in the same neuronal clusters, but not cells, as *Dagla*/*Daglb* (**Figure 4a2,b**). These data suggest that molecular and rate-limiting constituents of 2-AG signaling are present throughout neuronal diversification in the PVN, and could contribute to cell-state-specific intercellular communication, e.g., neuritogenesis[38,39].

 doi:10.20944/preprints202505.0066.v1



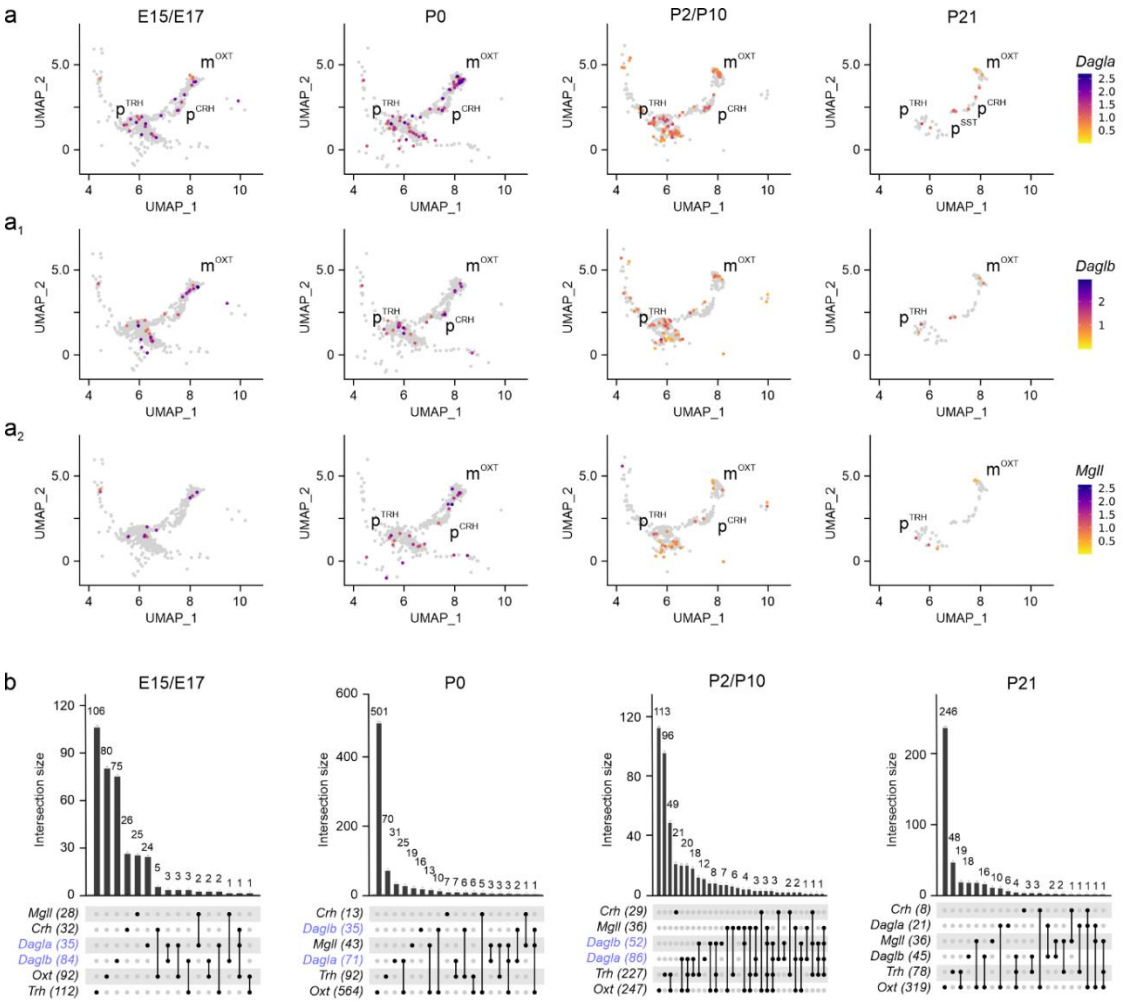


**Figure 4. *Dagla/b* and *Mgll* expression in the PVN.** (**a-a2**) UMAP representation in developing neurons showed *Dagla* << *Daglb* until birth (b, in blue), and *Mgll* at all time points. Relative expression was color-coded (to the right) for each gene analyzed. (**b**) *UpSet* plots showing gene enrichment and co-expression along brain development for the genes analyzed.

Subsequently, we determined the cellular foci for *Napepld* mRNA expression, implicated in AEA synthesis[40,41]. *Napepld* mRNA was sparse in both magnocellular and parvocellular PVN neurons at any time point (**Figure 5a,b**). In contrast, *Gde1* expression[42] was promiscuous and significant in all neuronal clusters (**Figure 5a1,b**). The expression of *Faah*, the enzyme chiefly degrading AEA[43], was pronounced (>500 mRNA molecules/cell) throughout brain development in both magnocellular and parvocellular neurons (**Figure 5a2,b**). These data suggest 2-AG signaling in the PVN could affect many more neurons, corroborating its proposed role as the primary endocannabinoid involved with both neuritogenesis and retrograde signaling[44].

 doi:10.20944/preprints202505.0066.v1



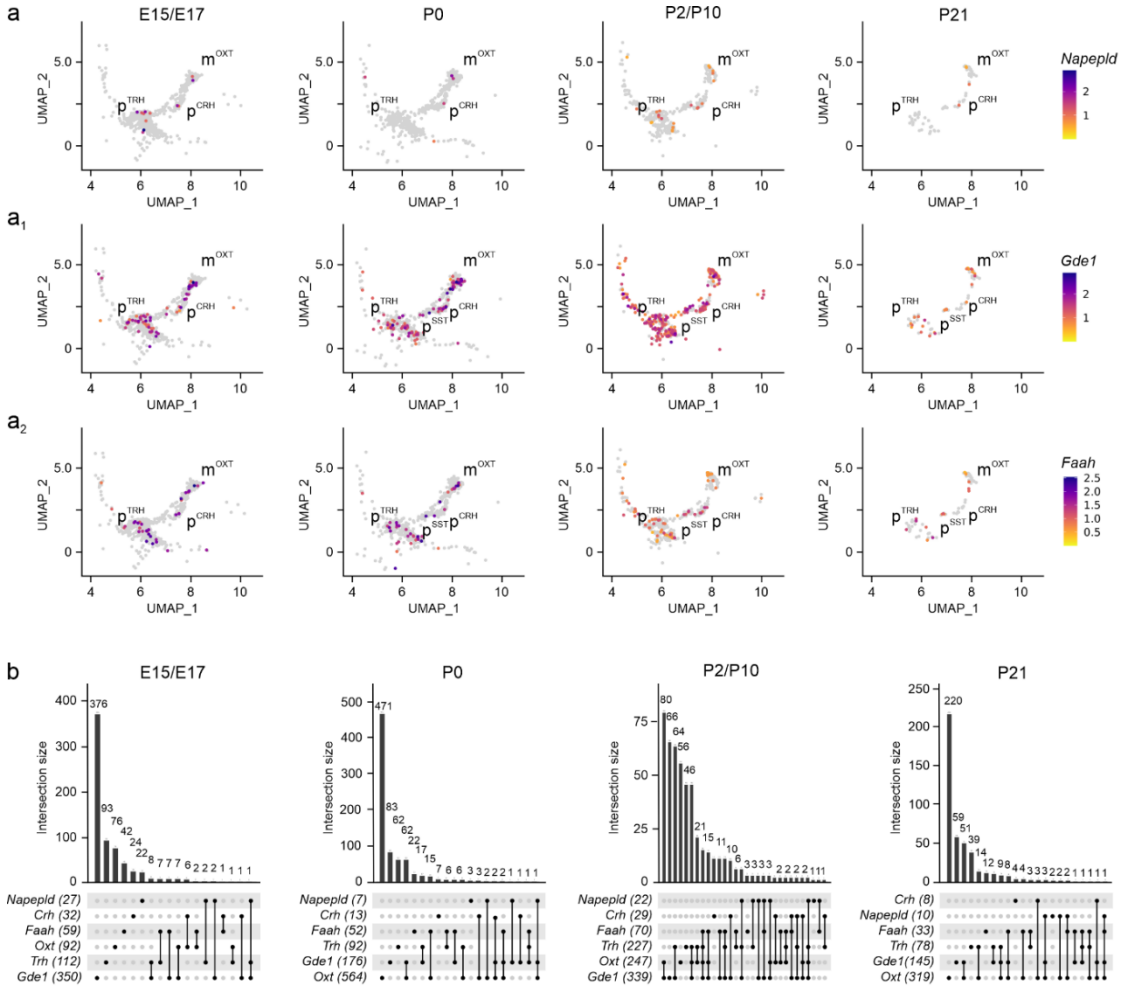


**Figure 5. *Napepld*, *Gde1*, and *Faah* expression in the PVN.** (**a-a**$_2$) UMAP representation of *Napepld*, *Gde1*, and *Faah* expression in neurons populating the PVN. Relative expression was color-coded (to the right) for each gene analyzed. (**b**) *UpSet* plots showing gene enrichment and co-expression along brain development for the genes analyzed.

**Nanoscale anatomy of 2-AG signaling revealed by in situ hybridization.** We have performed multiplexed fluorescence in situ hybridization to reconstruct 2-AG signaling, which appeared superior relative to AEA in the PVN (**Figure 6**). At E15.5, the prospective territory of the PVN was outlined by *Cnr1* mRNA expression, which reminisced the shape of the adult structure (**Figure 6a,a**$_1$ **vs. Figure 1b**): *Cnr1* mRNA localized to the majority of p$^{CRH}$ neurons (**Figure 6a**$_{1,2}$), alike to subpopulations of m$^{OXT}$ and p$^{TRH}$ neurons (**Figure 6a**$_{3,4}$). While *Daglb* mRNA transcripts were found in most p$^{CRH}$, m$^{OXT}$ and p$^{TRH}$ cells (**Figure 6a**$_{1\text{-}4}$), *Dagla* was not detected reliably by in situ hybridization at E15.5, even if we excluded technical frailties by visualizing *Dagla* in the hippocampus *en masse* during embryogenesis (**Figure S3a,b**). Thus, we continued with the analysis of *Daglb* for developmental stages and found *Daglb* mRNA abundantly at E15.5 (**Figure 6a**$_2$). At P10, both *Cnr1* and *Daglb* remained expressed in both p$^{TRH}$ and m$^{OXT}$ cells (**Figure 6b-c**$_1$). *Mgll* was present in m$^{OXT}$ neurons, and co-existed with *Cnr1* (**Figure 6c**$_1$**,c**$_1$). At P21, *Daglb* and *Mgll* were rarely expressed. In contrast, *Dagla* co-localized with *Cnr1* primarily in p$^{TRH}$ neurons (**Figure 6d-d**$_2$). Similarly, we continued to detect *Cnr1* mRNA in p$^{CRH}$ cells (**Figure 6e,e**$_1$).

Preprints.org (www.preprints.org) | NOT PEER-REVIEWED | Posted: 2 May 2025 doi:10.20944/preprints202505.0066.v1



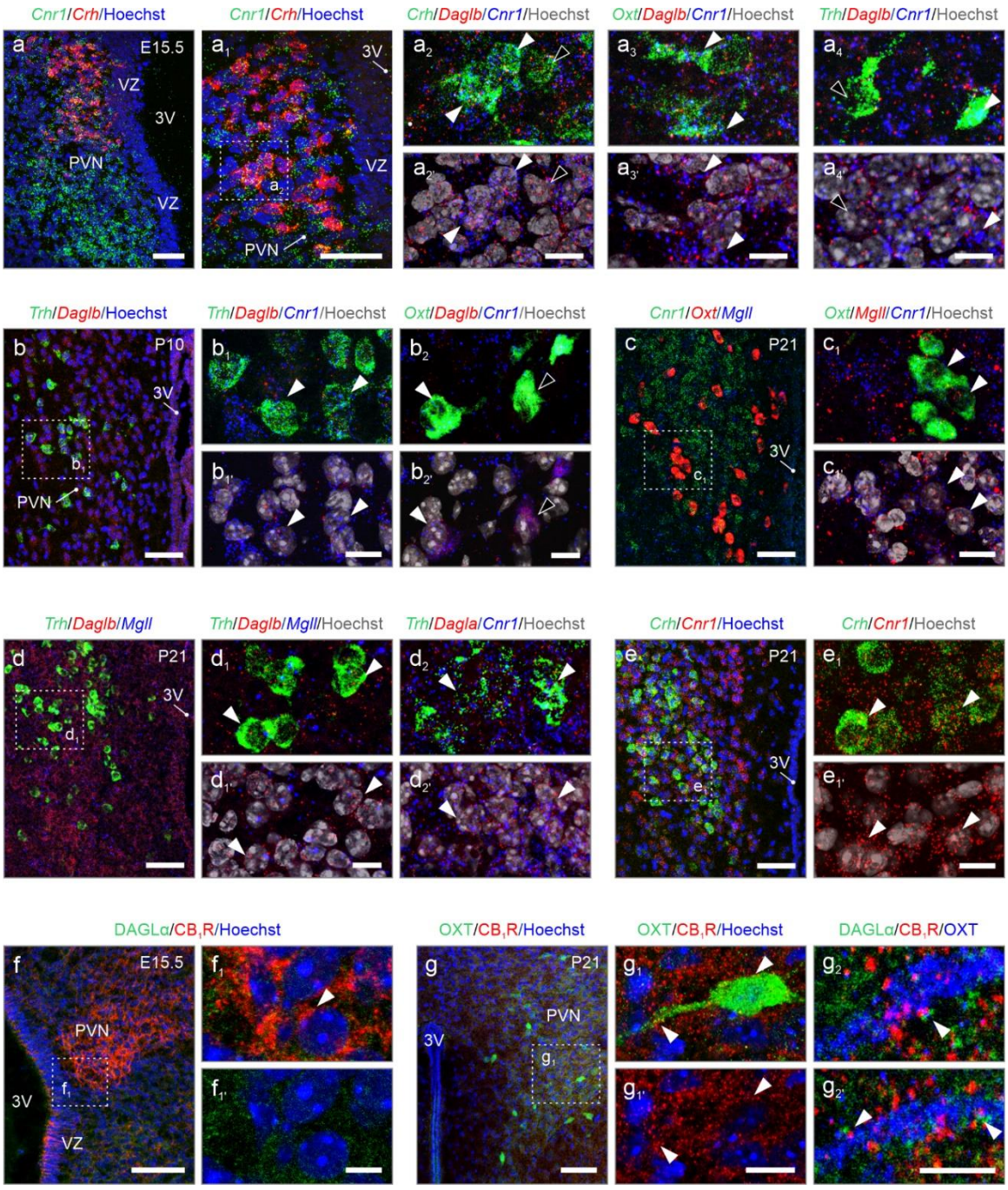


**Figure 6. Cell-type-specific localization of *Dagla, Daglb, Magll*, and** Cnr1 **by in situ hybrization.** (**a-a**$_4$) Already at E15.5, distinct neuronal populations expressed either *Cnr1* or *Daglb*, or both. (**b**) At postnatal day 10 (P10), both *Cnr1* and *Daglb* expression were maintained. (**c-e**$_1$) At P21, PVN neurons continued to express *Cnr1*, *Daglb*, and *Mgll*, along with noticeable levels of *Dagla* (d$_2$). (**f-g**$_2$) Immunohistochemistry revealed the focal accumulation of CB$_1$Rs in the PVN at E15.5, which remained unchanged until P21 (*arrowheads*, f$_1$ vs. g$_1$). DAGL$\alpha$ dominated at P21, when it frequently apposed CB$_1$Rs in the somata and processes of, e.g., m$^{OXT}$ neurons (*arrowheads*, g$_2$). *Scale bars* = 50 µm (a,a$_1$,b,c,d,e,f,g), 20 µm (g$_1$), 10 µm (a$_2$,a$_3$,a$_4$,b$_1$,b$_2$,c$_1$,d$_1$,d$_2$,e$_1$), 5 µm (f$_1$,g$_2$).

Subsequently, we performed immunohistochemistry for DAGL$\alpha$ and CB$_1$Rs at E15.5 and P21. In accord with our results using in situ hybridization, CB$_1$R protein accumulated in the fetal PVN, and decorated punctae and processes, which we have interpreted as labeling of growth cones and nascent synapses on afferent input. In contrast, DAGL$\alpha$ immunoreactivity was minimal (**Figure 6f-f**$_1$). At P21, CB$_1$Rs continued to decorate terminal-like punctae, encircling perikarya and processes of, e.g., m$^{OXT}$-containing neurons (**Figure 6g,g**$_1$), with DAGL$\alpha$ confined mostly along the dendrites of neurons and

 doi:10.20944/preprints202505.0066.v1



in apposition to $CB_1$Rs (**Figure 6g,g$_2$**). In sum, cell-resolved neuroanatomy confirmed cell identities, transcript switches for *Dagla* and *Daglb*, the developmental dynamics for *Cnr1* mRNA, and classical configuration of DAGL$\alpha$ and $CB_1$R for retrograde signaling at the protein level.

**The endocannabinoid system in astrocytes.** As endocannabinoid signaling is essential for neuron-to-astrocyte communication in multiple physiological processes[45–47], we addressed if cannabinoid receptors and enzymes related to endocannabinoid metabolism were expressed in astrocytes in the pre-adolescent PVN. We justify the choice of P21 by the postnatal window of astrocytogenesis and maturation that sequentially occur between P2-P14[48]. Thus, terminally-differentiated astrocytes that could reflect *bona fide* PVN-related signaling could be resolved starting at P21[48]. We subdivided astrocytes based on their prototypical markers: excitatory amino acid transporter 1 (*Slc1a3*)[49], glial fibrillary acidic protein (*Gfap*)[50], and aldehyde dehydrogenase 1 family member L1 (*Aldh1l1*)[51], which jointly defined a cellular cluster (**Figure 7a**). When plotting cannabinoid receptors, we found a near complete lack of *Cnr1*, *Cnr2* and *Gpr55* mRNA (**Figure 7b,c**), which was unexpected as functional $CB_1$Rs have previously been localized to hypothalamic nuclei other than the PVN[52], as well as also to extrahypothalamic regions[26,46,53,54]. Both *Dagla* and *Daglb* mRNA were found in subsets of astrocytes, while *Mgll* mRNA was present in a larger subset (**Figure 7b$_1$,c**). Despite *Gde1* being present in astrocytes, neither *Napepld* nor *Faah* could be detected reliably (**Figure 7b$_2$,c**). We validated the above data by in situ hybridization, which showed the lack of *Cnr1* mRNAs but the presence of *Dagla* (**Figure 7d,d$_1$**). Thus, astrocytes in the PVN could contribute to endocannabinoid metabolism and assist in shaping synaptic neurotransmission[55].

 doi:10.20944/preprints202505.0066.v1



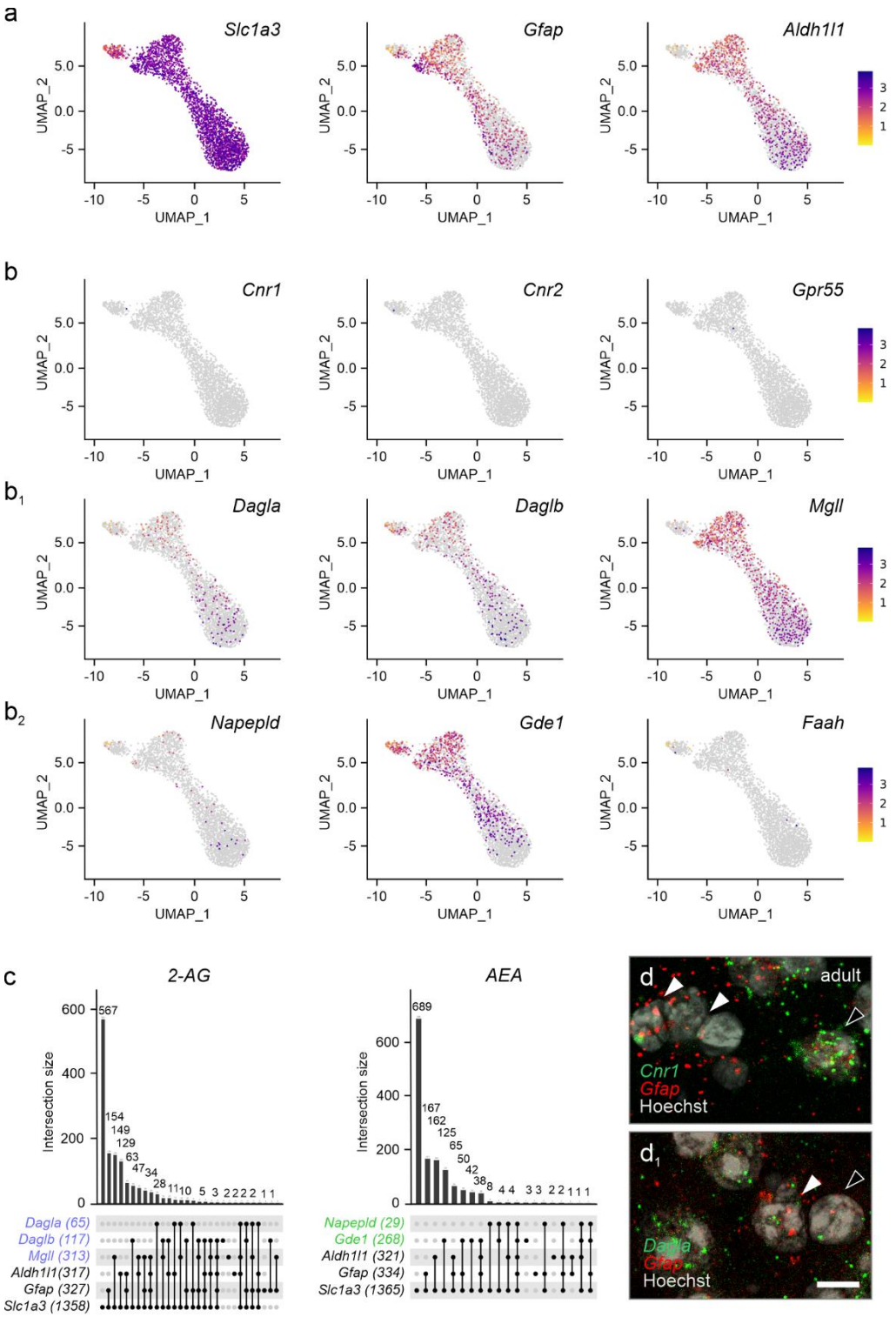


**Figure 7. Cannabinoid receptors and enzymes in astrocytes of the adult PVN.** (**a**) Gene set used to identify astrocytes. (**b-b**$_2$) Cannabinoid receptors (b), but not the machinery to control the bioavailability of 2-AG, were lacking in astrocytes. Relative expression was color-coded for each gene analyzed (to the right). (**c**) *UpSet* plots for gene enrichment in PVN astrocytes. Note the higher reliance on 2-AG signalling as compared to AEA (blue vs. green). (**d**) In situ hybridization confirmed the lack of *Cnr1* in *Gfap*$^+$ astrocytes (arrowheads indicate *Gfap*$^+$/*Cnr1*$^-$ astrocytes vs. open arrowheads denoting *Gfap*$^-$/*Cnr1*$^+$ cells, presumed neurons). (**d**$_1$) *Gfap*$^+$ astrocytes contained *Dagla* mRNA, even if at low abundance (*arrowheads*). *Scale bar* = 5 μm (d$_1$).

## 3. Discussion

 doi:10.20944/preprints202505.0066.v1



This study describes the developmental dynamics of cannabinoid receptor and endocannabinoid metabolism-related enzyme expression in the PVN of mice. Major findings include that all neurons go through a $CB_1R^+$ phase during embryonic and postnatal development, which is compatible with previous proposals on $CB_1R$ being ubiquitously expressed upon neurogenic commitment in vertebrates[38,56], and is associated with axonal growth and guidance. For 2-AG synthesis, our data recapitulates a developmentally regulated *Daglb*-to-*Dagla* switch, that has been shown for the cerebral cortex[57] but not the hypothalamus earlier. Moreover, the finding that *Daglb* and *Dagla*, but lower amounts of *Mgll*, are expressed in neurons of the PVN is compatible with known anatomical arrangements with the PVN being reliant on monosynaptic afferents from external sources (BNST, amygdala, arcuate nucleus, suprachiasmatic nucleus) rather than local interneurons to synchronize its endocrine output. Accordingly, MAGL, together with $CB_1Rs$, are expected to be expressed outside the PVN to time the presynaptic action of endocannabinoids produced by PVN neurons. Thus, the spatial configuration of endocannabinoid signaling during neuronal diversification in the PVN and in adulthood is adequate to control the avalanche of synaptic inputs arriving from intra- and extrahypothalamic areas. In addition, the importance of retrograde neurotransmission in the PVN is highlighted by the use of gaseous neuromodulators, particularly nitric oxide (NO). Neuronal NO synthase (*Nos1*) is particularly abundant in the PVN, as compared to other hypothalamic nuclei, and its effects on food intake[58,59], renal sympathetic nerve activity[60,61], and sympatho-adrenomedullary outflow[62] are well described.

Besides cannabinoid receptors, we mapped the cellular distribution of *Dagla, Daglb, Napepld, Gde1*, and *Faah*, enzymes that are fundamental to the turnover of endocannabinoids. Even though these enzymes are the most abundant to modulate endocannabinoid levels in the brain and at the periphery, we acknowledge the contributions of others that have not been studied: e.g., MGL degrades ~85% of 2-AG in the brain[63]. In contrast, α/β-hydrolase domain containing 6 (*Abhd6*)[64] and 12 (*Abhd12*)[65] account for ~4% and ~9% of 2-AG degradation, respectively[63]. Similarly, the metabolic pathway for AEA is complex, and includes *Abhd4, Gde4/7, Ptpn22*, as well as *Lox* and *Cox2*, for synthesis and degradation respectively (*for extensive reviews see* Refs.[66,67]). As the biological significance of these enzymes is less well understood, we did not pursue them in this report. We also note that *Gde1* has been found important to AEA synthesis, at least in vitro. Yet, AEA levels in the brain of $Gde1^{-/-}$ mice do not differ, questioning its role in AEA synthesis in vivo[68]. Therefore, and given the low abundance of *Napepld* mRNA expression, we hypothesize that 2-AG signaling might be more prevalent than AEA in the PVN. While we are confident that our study still provides substantial insights into the architecture of endocannabinoid signaling in the PVN, our datasets will certainly be amenable for further focused analysis if and when those aims are justified.

2-AG is considered to be the main circuit-breaker driving retrograde signaling in a fast, but phasic, manner[69,70], since 2-AG is a more potent agonist at the CB1R[71], is available at up to a 1,000-fold higher concentrations in the brain[18,69], and its absence curtails retrograde signaling in the DAGL$\alpha$ knockout mice[25]. Conversely, AEA is regarded as tonically inhibiting neuronal activity[44,70]. In accord with this hypothesis, previous reports suggest that tonic regulation of the HPA axis by AEA occurs either directly at neurons of the PVN[72] or indirectly through extrahypothalamic sites, such as the basolateral amygdala[44]. Nevertheless, mRNA levels predict neither protein abundance, nor enzymatic activity[73]. Therefore, cell-resolved electrophysiology will be best placed to define the contribution of these endocannabinoids to regulating specific behaviors.

While endocannabinoids limit neurotransmitter release through neuronal $CB_1Rs$, recent studies have proposed that $CB_1Rs$ on astrocytes could instead promote neuronal activity by controlling metabolite availability[27]. Accordingly, activation of mitochondrial $CB_1Rs$ in astrocytes could regulate glucose metabolism to ensure neuronal bioenergetics[53]. Furthermore, $CB_1Rs$ localized to astrocyte leaflets ensheathing blood vessels in the nucleus accumbens were implicated in regulating anxiety and depression-like behaviors[54]. In the hypothalamus, engagement of $CB_1Rs$ on or in astrocytes might regulate processes involved with energy metabolism, including leptin signaling and

 doi:10.20944/preprints202505.0066.v1



glycogen storage[52]. Therefore, we expected astrocytes in the PVN to express CB1Rs (and probably also others). Nevertheless, we could not detect any with the tools available this time. We did however find substantial expression of both DAGL isoforms, implicating astrocytes in 2-AG metabolism. As 2-AG can be released by astrocytes in response to other non-endocannabinoid-mediated signals, such as ATP[74], we propose that astrocytes could tune neuronal activity through $CB_1R$-independent 2-AG release. Thus, our findings suggest novel, metabolism-driven endocannabinoid availability as a potential rate-limiting step for the processing of synaptic inputs and translating those into hormonal output at the level of PVN neurons.

## 4. Materials and Methods

**Ethical considerations.** Mice were housed under standard husbandry conditions in a temperature and humidity-controlled room (12h/12h light cycle, 55% humidity, 22-24 $^{o}$C ambient temperature). Animals had *ad libitum* access to food and water throughout. The maintenance and welfare of the animals conformed to the 2010/63/European Communities Council directive. Experimental protocols for tissue collection were approved by the Austrian Ministry of Science and Research (66.009/0145-WF/II/3b/2014 and 66.009/0277-WF/V3b/2017). Pregnant (embryonic day (E) 15.5), and postnatal day (P) 4, P10, and P21 C57BL/6JRj mice were obtained from Janvier Labs and kept on site as adequate.

**Single-Cell RNA-seq data acquisition, and harmonization.** This study utilized two publicly available single-cell RNA-seq datasets to examine the expressional dynamics of genes related to endocannabinoid signaling during mouse hypothalamus development. The principal dataset comprised 51,199 cells, 24,340 features, and encompassed all developmental stages[15]. A second dataset was obtained as a pre-processed AnnData object, and contained 128,006 cells profiled for 27,998 genes along complementary developmental time points[29,75]. All subsequent analyses were performed in *R* (version 4.3 or higher) within a reproducible workflow framework documented using Quarto notebooks[76]. Gene expression matrices were appropriately transposed, and cell/gene metadata were standardized. Uniform Manifold Approximation and Projection (UMAP) coordinates within the dataset were integrated as distinct dimensionality reduction objects within Seurat[77–79]. Metadata pertaining to developmental stages and original cluster annotations were preserved. The Romanov *et al*.[15] dataset, available as a Seurat RDS file, was loaded and updated to the latest Seurat object specifications. Cluster identities and associated colour palettes were harmonized across both datasets to facilitate comparative analyses.

**Cellular quality control and filtering.** Stringent quality control was performed on both datasets to exclude potentially compromised cells and technical artefacts. Cells were retained if they had more than 500 unique genes and fewer than 25,000 unique molecular identifiers (UMIs). Additional filtering excluded cells based on high percentages of mitochondrial, ribosomal, or hemoglobin genes, elevated doublet prediction scores, and low transcriptomic complexity (log10 genes per UMI). These thresholds were enforced to enrich high-quality cellular profiles while acknowledging the potential exclusion of certain biological states, as per any filtering strategy[15,80].

**Gene set curation and expression analysis.** Gene sets representing canonical endocannabinoid receptors (*Cnr1, Cnr2, Gpr55*), metabolic enzymes (*Dagla, Daglb, Gde1, Mgll, Napepld, Faah*), and neuropeptides pertinent to hypothalamic classification (*Oxt, Avp, Crh, Sst, Trh*) were defined based on established literature[19,81–84]. To focus analyses on more robustly expressed genes and to mitigate noise from sparse detection, expression matrices were filtered to include only genes ranking above the 40th percentile of mean expression across all cells. For qualitative assessment of co-expression, gene expression was binarized based on detection status (expression > 0.5th percentile for each gene separately) within individual cells. Therefore, intersectional co-expression patterns among key gene sets could be visualized using *UpSet* plots generated with the *UpSetR* package[80,85]. UMAP was used to visualize high-dimensional cellular states in two dimensions, primarily using coordinates provided in the original datasets or recomputed as necessary[15,29,78–80]. The expression patterns of specific genes and the aggregate expression of curated gene sets were

 doi:10.20944/preprints202505.0066.v1



visualized across developmental stages and cell clusters using Seurat's *FeaturePlot* function, optimizing parameters such as point size and transparency for clarity[77].

**Descriptive statistics and exploratory analysis.** Quantitative summaries of gene expression, including mean, standard deviation, and quartiles, were calculated for the specified target genes at the developmental periods indicated. The *skimr* package was used for descriptive statistics for numerical metadata and expression features, ensuring transparency regarding data distributions and completeness[80].

**In situ hybridization:** Embryonic heads (E15.5) and extracted brains (P10, P21) were rapidly frozen on dry-ice in plastic moulds filled with optimal cutting medium (O.C.T; Sakura), and cryosectioned at 16-µm thickness on a Leica CM1860 cryostat microtome. Coronal sections containing the PVN were collected serially on SuperFrost⁺ glass slides (ThermoFisher), air-dried for 20 min, and stored at -80 °C until processing. Tissue sections were immersion fixed in 4% paraformaldehyde (PFA) in 0.05M phosphate buffered-saline (PBS, pH 7.4) at 4 °C for 20 min, rinsed in PBS, and subsequently dehydrated in an ascending gradient of ethanol (25%, 50%, 75%, and 100%, 5 min each). In situ hybridization was multiplexed according to the HCR v3.0 protocol for '*generic sample on slide*' with probe sets combining *Slc32a1*, *Crh*, *Trh*, *Oxt*, *Cnr1*, *Dagla*, *Daglb*, and *Mgll* (all from Molecular Instruments). Sections were counterstained with Hoechst 33,342 (Sigma Aldrich) and mounted with Entellan (Merck). Sections with two or more colours from appropriately labelled hairpin combinations were imaged on an LSM880 confocal microscope (Zeiss; pinhole set to 1 airy unit, and minimal laser power [<5% per channel]; 20x/0.8 NA objective for survey images and Plan-Apochromat 63x/1.4 N.A. objective for high-resolution images), processed with the ZEN software (Zeiss), and compiled as multi-panel images in CorelDRAW 2022 (Corel Corp.).

**Immunohistochemistry.** Whole heads of mouse foetuses (E15.5) were immersion fixed overnight with 4% PFA in 0.05M PBS at 4 °C before cryoprotection in 30% sucrose in 0.05M PBS. P21 mice were transcardially perfused with 4% PFA in 0.1M phosphate buffer (PB, pH 7.4), with their brains removed and post-fixed at 4 °C overnight, before cryoprotection in 30% sucrose in 0.05M PBS. Tissues were rapidly frozen and cryosectioned on a Leica CM1860 cryostat at either 20 µm (E15.5) and collected on SuperFrost⁺ glass slides (Thermo Fisher) or 50 µm for free-floating labelling (P21). Next, sections were incubated with a blocking solution containing 5% normal donkey serum (NDS, Jackson ImmunoResearch), 2% bovine serum albumin (BSA, Sigma) and 0.2% Triton X-100 (Sigma) in PBS at room temperature for 1h to block non-specific binding. Tissues were subsequently exposed to a combination of primary antibodies (guinea pig anti-$CB_1R$ [Af530], 1:500, Nittobo Medical; goat anti-DAGL$\alpha$ [Af1080], 1:500, Nittobo Medical, and rabbit anti-oxytocin [AB911], 1:1,000; Merck Millipore) diluted in 2% NDS, 0.1% BSA, 0.2% Triton X-100 in PBS at 4 °C for 72h. After extensive rinsing in PBS, appropriate combinations of secondary IgGs conjugated with carbocyanine (Cy)2, 3 or 5 (raised in donkey, 1:300, Jackson ImmunoResearch) were applied at 22-24 °C for 2h. Sections were counterstained with Hoechst 33,342 (Sigma Aldrich) to visualize nuclei. After extensive washing in PBS, sections were rinsed in distilled water, air-dried, and cover slipped with Entellan (in xylene, Sigma-Aldrich).

**Supplementary Materials:** The following supporting information can be downloaded at the website of this paper posted on Preprints.org.

**Author Contributions statement:** E.T. and T.H. defined the scope of this study. E.T., Z.H., C.B., A.A., and E.K. performed experiments and analyzed data. E.K. and T.H. wrote the manuscript.

**Funding statement:** This work was supported by the Austrian Science Fund (FWF, P 34121-B to E.K.; COE-16B to T.H.), the Swedish Research Council (2023-03058, T.H.), the Novo Nordisk Foundation (NNF23OC0084476, to T.H.), the European Research Council (FOODFORLIFE, ERC-2020-AdG-101021016; to T.H.), the National Brain Research Program of Hungary (NAP2022-I-1/2022 to A.A.) and the Excellence Program for Higher Education of Hungary (TKP-EGA-25, to A.A.).

**Code availability:** Analysis of RNA-seq data relied on published protocols[15].

 doi:10.20944/preprints202505.0066.v1



**Data availability:** The snRNA-seq data generated in this study have been deposited in the NCBI Gene Expression Omnibus database under accession code (GSE132730). All primary data were made publicly available at https://github.com/EugOT/eCB-hypothalamus-development and deposited to Figshare.com with DOI: 10.6084/m9.figshare.28816100. All other relevant data were included in the figures.

**Competing interests statement:** The authors of this manuscript declare no conflict of interest.

## References


1. Fong, H., Zheng, J. & Kurrasch, D. The structural and functional complexity of the integrative hypothalamus. *Science* **382**, 388–394 (2023).
2. Qin, C., Li, J. & Tang, K. The Paraventricular Nucleus of the Hypothalamus: Development, Function, and Human Diseases. *Endocrinology* **159**, 3458–3472 (2018).
3. Ben-Shlomo, A. & Melmed, S. Pituitary Somatostatin Receptor Signaling. *Trends Endocrinol Metab* **21**, 123–133 (2010).
4. Wang, J. et al. Role and mechanism of PVN-sympathetic-adipose circuit in depression and insulin resistance induced by chronic stress. *EMBO Rep* **24**, e57176 (2023).
5. Li, Y.-J. et al. Paraventricular nucleus-central amygdala oxytocinergic projection modulates pain-related anxiety-like behaviors in mice. *CNS Neurosci Ther* **29**, 3493–3506 (2023).
6. Fenselau, H. et al. A rapidly acting glutamatergic ARC→PVH satiety circuit postsynaptically regulated by $\alpha$-MSH. *Nat Neurosci* **20**, 42–51 (2017).
7. Krashes, M. J., Shah, B. P., Koda, S. & Lowell, B. B. Rapid versus Delayed Stimulation of Feeding by the Endogenously Released AgRP Neuron Mediators GABA, NPY, and AgRP. *Cell Metabolism* **18**, 588–595 (2013).
8. Cowley, M. A. et al. Leptin activates anorexigenic POMC neurons through a neural network in the arcuate nucleus. *Nature* **411**, 480–484 (2001).
9. Caron, A. et al. POMC neurons expressing leptin receptors coordinate metabolic responses to fasting via suppression of leptin levels. *eLife* **7**, e33710.
10. Kondoh, K. et al. A specific area of olfactory cortex involved in stress hormone responses to predator odours. *Nature* **532**, 103–106 (2016).
11. Kaouane, N., Ada, S., Hausleitner, M. & Haubensak, W. Dorsal Bed Nucleus of the Stria Terminalis-Subcortical Output Circuits Encode Positive Bias in Pavlovian Fear and Reward. *Front Neural Circuits* **15**, 772512 (2021).
12. Decavel, C. & Van Den Pol, A. N. GABA: A dominant neurotransmitter in the hypothalamus. *Journal of Comparative Neurology* **302**, 1019–1037 (1990).
13. Mendonça, M. M. et al. Involvement of GABAergic and Adrenergic Neurotransmissions on Paraventricular Nucleus of Hypothalamus in the Control of Cardiac Function. *Front. Physiol.* **9**, (2018).
14. Li, Y.-F., Jackson, K. L., Stern, J. E., Rabeler, B. & Patel, K. P. Interaction between glutamate and GABA systems in the integration of sympathetic outflow by the paraventricular nucleus of the hypothalamus. *American Journal of Physiology-Heart and Circulatory Physiology* **291**, H2847–H2856 (2006).
15. Romanov, R. A. et al. Molecular design of hypothalamus development. *Nature* 1–7 (2020) doi:10.1038/s41586-020-2266-0.
16. Matsuda, L. A., Lolait, S. J., Brownstein, M. J., Young, A. C. & Bonner, T. I. Structure of a cannabinoid receptor and functional expression of the cloned cDNA. *Nature* **346**, 561–564 (1990).
17. Mechoulam, R. et al. Identification of an endogenous 2-monoglyceride, present in canine gut, that binds to cannabinoid receptors. *Biochem. Pharmacol.* **50**, 83–90 (1995).
18. Stella, N., Schweitzer, P. & Piomelli, D. A second endogenous cannabinoid that modulates long-term potentiation. *Nature* **388**, 773–778 (1997).
19. Kano, M., Ohno-Shosaku, T., Hashimotodani, Y., Uchigashima, M. & Watanabe, M. Endocannabinoid-mediated control of synaptic transmission. *Physiol. Rev.* **89**, 309–380 (2009).
20. Cardinal, P. et al. Cannabinoid type 1 (CB1) receptors on Sim1-expressing neurons regulate energy expenditure in male mice. *Endocrinology* **156**, 411–418 (2015).

 doi:10.20944/preprints202505.0066.v1




21. Mazier, W. et al. mTORC1 and CB1 receptor signaling regulate excitatory glutamatergic inputs onto the hypothalamic paraventricular nucleus in response to energy availability. *Mol Metab* **28**, 151–159 (2019).
22. Cruz-Martínez, A. M. et al. CB1 receptors in the paraventricular nucleus of the hypothalamus modulate the release of 5-HT and GABA to stimulate food intake in rats. *Eur Neuropsychopharmacol* **28**, 1247–1259 (2018).
23. Petrie, G. N. et al. Disruption of tonic endocannabinoid signalling triggers cellular, behavioural and neuroendocrine responses consistent with a stress response. *Br J Pharmacol* **180**, 3146–3159 (2023).
24. Gorzalka, B. B. & Hill, M. N. Integration of endocannabinoid signaling into the neural network regulating stress-induced activation of the hypothalamic-pituitary-adrenal axis. *Curr Top Behav Neurosci* **1**, 289–306 (2009).
25. Tanimura, A. et al. The endocannabinoid 2-arachidonoylglycerol produced by diacylglycerol lipase alpha mediates retrograde suppression of synaptic transmission. *Neuron* **65**, 320–327 (2010).
26. Navarrete, M. & Araque, A. Endocannabinoids Mediate Neuron-Astrocyte Communication. *Neuron* **57**, 883–893 (2008).
27. Navarrete, M. & Araque, A. Endocannabinoids Potentiate Synaptic Transmission through Stimulation of Astrocytes. *Neuron* **68**, 113–126 (2010).
28. Ivell, R. & Richter, D. Structure and comparison of the oxytocin and vasopressin genes from rat. *Proceedings of the National Academy of Sciences* **81**, 2006–2010 (1984).
29. Kim, D. W. et al. The cellular and molecular landscape of hypothalamic patterning and differentiation from embryonic to late postnatal development. *Nat Commun* **11**, 4360 (2020).
30. Munro, S., Thomas, K. L. & Abu-Shaar, M. Molecular characterization of a peripheral receptor for cannabinoids. *Nature* **365**, 61–65 (1993).
31. Lauckner, J. E. et al. GPR55 is a cannabinoid receptor that increases intracellular calcium and inhibits M current. *Proc. Natl. Acad. Sci. U.S.A.* **105**, 2699–2704 (2008).
32. Grabon, W. et al. CB2 expression in mouse brain: from mapping to regulation in microglia under inflammatory conditions. *Journal of Neuroinflammation* **21**, 206 (2024).
33. Cherif, H. et al. Role of GPR55 during Axon Growth and Target Innervation. *eNeuro* **2**, (2015).
34. Harkany, T., Mackie, K. & Doherty, P. Wiring and firing neuronal networks: endocannabinoids take center stage. *Curr Opin Neurobiol* **18**, 338–345 (2008).
35. Bisogno, T. et al. Cloning of the first sn1-DAG lipases points to the spatial and temporal regulation of endocannabinoid signaling in the brain. *J. Cell Biol.* **163**, 463–468 (2003).
36. Dinh, T. P. et al. Brain monoglyceride lipase participating in endocannabinoid inactivation. *Proc Natl Acad Sci U S A* **99**, 10819–10824 (2002).
37. Oudin, M. J., Hobbs, C. & Doherty, P. DAGL-dependent endocannabinoid signalling: roles in axonal pathfinding, synaptic plasticity and adult neurogenesis. *Eur. J. Neurosci.* **34**, 1634–1646 (2011).
38. Mulder, J. et al. Endocannabinoid signaling controls pyramidal cell specification and long-range axon patterning. *Proc. Natl. Acad. Sci. U.S.A.* **105**, 8760–8765 (2008).
39. Keimpema, E. et al. Diacylglycerol lipase alpha manipulation reveals developmental roles for intercellular endocannabinoid signaling. *Scientific reports* **3**, 2093 (2013).
40. Okamoto, Y., Morishita, J., Tsuboi, K., Tonai, T. & Ueda, N. Molecular Characterization of a Phospholipase D Generating Anandamide and Its Congeners*. *Journal of Biological Chemistry* **279**, 5298–5305 (2004).
41. Leishman, E., Mackie, K., Luquet, S. & Bradshaw, H. B. Lipidomics profile of a NAPE-PLD KO mouse provides evidence of a broader role of this enzyme in lipid metabolism in the brain. *Biochim Biophys Acta* **1861**, 491–500 (2016).
42. Simon, G. M. & Cravatt, B. F. Anandamide Biosynthesis Catalyzed by the Phosphodiesterase GDE1 and Detection of Glycerophospho-*N*-acyl Ethanolamine Precursors in Mouse Brain*. *Journal of Biological Chemistry* **283**, 9341–9349 (2008).
43. Deutsch, D. G. & Chin, S. A. Enzymatic synthesis and degradation of anandamide, a cannabinoid receptor agonist. *Biochem Pharmacol* **46**, 791–796 (1993).
44. Hill, M. N. & Tasker, J. G. Endocannabinoid Signaling, Glucocorticoid-Mediated Negative Feedback and Regulation of the HPA Axis. *Neuroscience* **204**, 5–16 (2012).

 doi:10.20944/preprints202505.0066.v1




45. Coiret, G. et al. Neuron to astrocyte communication via cannabinoid receptors is necessary for sustained epileptiform activity in rat hippocampus. *PLoS One* **7**, e37320 (2012).
46. Eraso-Pichot, A. et al. Endocannabinoid signaling in astrocytes. *Glia* **71**, 44–59 (2023).
47. Hebert-Chatelain, E. et al. A cannabinoid link between mitochondria and memory. *Nature* **539**, 555–559 (2016).
48. Akdemir, E. S., Huang, A. Y.-S. & Deneen, B. Astrocytogenesis: where, when, and how. *F1000Res* **9**, F1000 Faculty Rev-233 (2020).
49. Rothstein, J. D. et al. Localization of neuronal and glial glutamate transporters. *Neuron* **13**, 713–725 (1994).
50. Jacque, C. M. et al. Determination of glial fibrillary acidic protein (GFAP) in human brain tumors. *Journal of the Neurological Sciences* **35**, 147–155 (1978).
51. Cahoy, J. D. et al. A Transcriptome Database for Astrocytes, Neurons, and Oligodendrocytes: A New Resource for Understanding Brain Development and Function. *J. Neurosci.* **28**, 264–278 (2008).
52. Bosier, B. et al. Astroglial CB1 cannabinoid receptors regulate leptin signaling in mouse brain astrocytes. *Molecular Metabolism* **2**, 393–404 (2013).
53. Jimenez-Blasco, D. et al. Glucose metabolism links astroglial mitochondria to cannabinoid effects. *Nature* **583**, 603–608 (2020).
54. Dudek, K. A. et al. Astrocytic cannabinoid receptor 1 promotes resilience by dampening stress-induced blood-brain barrier alterations. *Nat Neurosci* **28**, 766–782 (2025).
55. Moro Chao, D. H. et al. Hypothalamic astrocytes control systemic glucose metabolism and energy balance. *Cell Metab* **34**, 1532-1547.e6 (2022).
56. Begbie, J., Doherty, P. & Graham, A. Cannabinoid receptor, CB1, expression follows neuronal differentiation in the early chick embryo. *J Anat* **205**, 213–218 (2004).
57. Gao, Y. et al. Loss of Retrograde Endocannabinoid Signaling and Reduced Adult Neurogenesis in Diacylglycerol Lipase Knock-out Mice. *J. Neurosci.* **30**, 2017–2024 (2010).
58. Zaia, C. T. B. V. et al. Vasoactive intestinal peptide promotes hypophagia and metabolic changes: Role of paraventricular hypothalamic nucleus and nitric oxide. *Brain Research Bulletin* **189**, 102–110 (2022).
59. Abtahi, S., Mirza, A., Howell, E. & Currie, P. J. Ghrelin enhances food intake and carbohydrate oxidation in a nitric oxide dependent manner. *General and Comparative Endocrinology* **250**, 9–14 (2017).
60. Zhang, K., Mayhan, W. G. & Patel, K. P. Nitric oxide within the paraventricular nucleus mediates changes in renal sympathetic nerve activity. *Am J Physiol* **273**, R864-872 (1997).
61. McBryde, F. D., Liu, B. H., Roloff, E. V., Kasparov, S. & Paton, J. F. R. Hypothalamic paraventricular nucleus neuronal nitric oxide synthase activity is a major determinant of renal sympathetic discharge in conscious Wistar rats. *Experimental Physiology* **103**, 419–428 (2018).
62. Yamaguchi, N., Okada, S., Usui, D. & Yokotani, K. Nitric oxide synthase isozymes in spinally projecting PVN neurons are involved in CRF-induced sympathetic activation. *Autonomic Neuroscience* **148**, 83–89 (2009).
63. Savinainen, J. R., Saario, S. M. & Laitinen, J. T. The serine hydrolases MAGL, ABHD6 and ABHD12 as guardians of 2-arachidonoylglycerol signalling through cannabinoid receptors. *Acta Physiol (Oxf)* **204**, 267–276 (2012).
64. Marrs, W. R. et al. The serine hydrolase ABHD6 controls the accumulation and efficacy of 2-AG at cannabinoid receptors. *Nat Neurosci* **13**, 951–957 (2010).
65. Blankman, J. L., Simon, G. M. & Cravatt, B. F. A Comprehensive Profile of Brain Enzymes that Hydrolyze the Endocannabinoid 2-Arachidonoylglycerol. *Chemistry & Biology* **14**, 1347–1356 (2007).
66. Maccarrone, M. Metabolism of the Endocannabinoid Anandamide: Open Questions after 25 Years. *Front. Mol. Neurosci.* **10**, (2017).
67. Simard, M. et al. Biosynthesis and metabolism of endocannabinoids and their congeners from the monoacylglycerol and *N*-acyl-ethanolamine families. *Biochemical Pharmacology* **205**, 115261 (2022).
68. Simon, G. M. & Cravatt, B. F. Characterization of mice lacking candidate N-acyl ethanolamine biosynthetic enzymes provides evidence for multiple pathways that contribute to endocannabinoid production in vivo. *Mol. BioSyst.* **6**, 1411–1418 (2010).

 doi:10.20944/preprints202505.0066.v1




69. Buczynski, M. W. & Parsons, L. H. Quantification of brain endocannabinoid levels: methods, interpretations and pitfalls. *Br J Pharmacol* **160**, 423–442 (2010).
70. Ohno-Shosaku, T. & Kano, M. Endocannabinoid-mediated retrograde modulation of synaptic transmission. *Current Opinion in Neurobiology* **29**, 1–8 (2014).
71. Savinainen, J. R., Järvinen, T., Laine, K. & Laitinen, J. T. Despite substantial degradation, 2-arachidonoylglycerol is a potent full efficacy agonist mediating CB1 receptor-dependent G-protein activation in rat cerebellar membranes. *British Journal of Pharmacology* **134**, 664–672 (2001).
72. Chapman, C. D. et al. Paraventricular nucleus anandamide signaling alters eating and substrate oxidation. *Neuroreport* **23**, 425–429 (2012).
73. Abruzzese, F., Greco, M., Perlino, E., Doonan, S. & Marra, E. Lack of correlation between mRNA expression and enzymatic activity of the aspartate aminotransferase isoenzymes in various tissues of the rat. *FEBS Lett* **366**, 170–172 (1995).
74. Walter, L., Dinh, T. & Stella, N. ATP induces a rapid and pronounced increase in 2-arachidonoylglycerol production by astrocytes, a response limited by monoacylglycerol lipase. *J Neurosci* **24**, 8068–8074 (2004).
75. Virshup, I., Rybakov, S., Theis, F. J., Angerer, P. & Wolf, F. A. anndata: Access and store annotated datamatrices. *JOSS* **9**, 4371 (2024).
76. Blischak, J., Carbonetto, P. & Stephens, M. Creating and Sharing Reproducible Research Code the Workflowr Way. *F1000research* (2019) doi:10.12688/f1000research.20843.1.
77. Hao, Y. et al. Integrated analysis of multimodal single-cell data. *Cell* (2021) doi:10.1016/j.cell.2021.04.048.
78. McInnes, L., Healy, J., Saul, N. & Großberger, L. UMAP: Uniform Manifold Approximation and Projection. *JOSS* **3**, 861 (2018).
79. Kobak, D. & Linderman, G. C. Initialization is critical for preserving global data structure in both t-SNE and UMAP. *Nat Biotechnol* **39**, 156–157 (2021).
80. Zupančič, M. et al. Concerted transcriptional regulation of the morphogenesis of hypothalamic neurons by ONECUT3. *Nat Commun* **15**, 8631 (2024).
81. Simmons, D. M. & Swanson, L. W. Comparison of the spatial distribution of seven types of neuroendocrine neurons in the rat paraventricular nucleus: toward a global 3D model. *J Comp Neurol* **516**, 423–441 (2009).
82. Romanov, R. A. & Harkany, T. Neuronal heterogeneity in the paraventricular nucleus of the hypothalamus as revealed by single-cell RNA-seq. *Current Opinion in Endocrine and Metabolic Research* **25**, 100366 (2022).
83. Keimpema, E., Di Marzo, V. & Harkany, T. Biological basis of cannabinoid medicines. *Science* **374**, 1449–1450 (2021).
84. Maccarrone, M., Guzmán, M., Mackie, K., Doherty, P. & Harkany, T. Programming of neural cells by (endo)cannabinoids: from physiological rules to emerging therapies. *Nat Rev Neurosci* **15**, 786–801 (2014).
85. Conway, J. R., Lex, A. & Gehlenborg, N. UpSetR: an R package for the visualization of intersecting sets and their properties. *Bioinformatics* **33**, 2938–2940 (2017).